ORIGINAL ARTICLES

An Investigation of Effect of Stand-Off Distance on the Material Removal Characteristics and Surface Generation in Fluid Jet Polishing

Chun Jin Wang[1] (ORCID) · **Chi Fai Cheung**[1] · **Lai Ting Ho**[1] · **Yee Man Loh**[1]

Abstract

Fluid jet polishing (FJP) is a versatile polishing process that has many advantages compared to other polishing processes. Stand-off distance (SOD) is one of the key parameters in fluid jet polishing. However, relatively little research work has been carried out to investigate its effect of SOD on material removal characteristics and surface generation in FJP. In this paper, a systematic investigation of the effect of SOD on the tool influence function and surface topography in FJP was conducted. Experiments were designed for FJP two kinds of materials corresponding to ductile and brittle materials. They are nickel copper (NiCu) alloy and BK7 optical glass, respectively. In this study, the SOD was varied from 2 to 35 mm. Analysis and discussions were made on its effect on the shape of TIF, material removal rate, and surface topography. It is interesting to note that the TIF shape becomes a Gaussian-like shape with large SOD both on NiCu and BK7, which provides a novel way to optimize the TIF in FJP. The variation of the material removal rate and surface roughness versus SOD on NiCu and BK7 were also determined from the experimental results. Moreover, the surface topography of NiCu and BK7 were characterized from the results measured from the white light interferometer and scan electron microscope. The outcome of the study provides a better understanding of the material removal characteristics and surface generation mechanism in FJP.

Keywords Fluid jet polishing · Material removal characteristics · Stand-off distance · Tool influence function · Surface generation · Ultra-precision machining

1 Introduction

Fluid jet polishing (FJP) [1, 2] is a versatile polishing process, which is a kind of working mode of the abrasive water jet machining process [3–5] with a working fluid pressure of less than 20 bar [6]. It is also a non-contact polishing process [7], which is beneficial for the polishing of freeform surfaces. Fähnle et al. [1] firstly used this method for polishing optical lens. In FJP, abrasives and water are mixed adequately by mechanical stirring in a tank, and pumped at a low pressure to a nozzle, as shown in Fig. 1a. The generated jet impinges the target surface vertically leading to material removal, as shown in Fig. 1b. Compared to traditional polishing methods, FJP has many advantages, including the

ability to polish various freeform surfaces, less tool wear and temperature increase during the polishing process, the ability to generate small tool influence functions (TIF) to dramatically reduce the edge effect, and a wide range of material removal rates through controlling the polishing parameters [2, 3, 6]. Hence, it has become an appealing method for polishing freeform surfaces for a number of materials, and an increasing amount of attention has been paid to this promising polishing process.

After the development of FJP, Fähnle et al. [8–10] and Booij et al. [11] started to do a series of research on material removal characterization and experimental optimization of the polishing process of optical lenses. Fang et al. [12, 13] studied the surface roughness, material removal, and edge effect of the FJP process. Tsai et al. [14] designed a Taguchi experiment to investigate and optimize the FJP polishing conditions when SKD61 mold steel is polished. Zhu et al. [15] did a series of experimental studies focusing on polishing hard-brittle materials after FJP. Li et al. [16, 17] optimized the tool influence function (TIF) of FJP so as to obtain Gaussian-like shape TIF for corrective polishing, and

✉ Chun Jin Wang
chunjin.wang@polyu.edu.hk

1 State Key Laboratory of Ultra-precision Machining Technology, Department of Industrial and Systems Engineering, The Hong Kong Polytechnic University, Hung Hom, Kowloon, Hong Kong, China
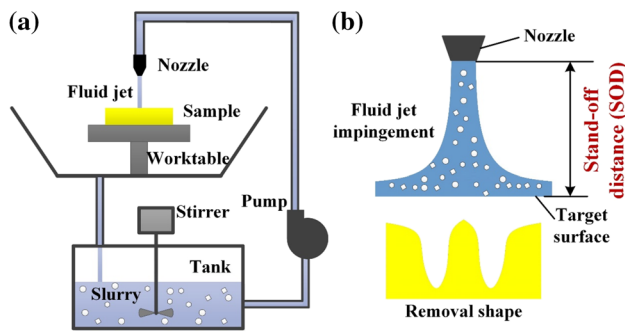
Fig. 1 Schematic diagram of fluid jet polishing system. **a** Illustration of the system, and **b** vertical jet impingement and its material removal shape

adopted FJP to remove the tool marks left on single-point diamond turning. Beaucamp et al. [6] proposed a computational fluid dynamics model for FJP based on multiphase turbulent flow computational method, which is able to achieve arithmetic roughness (R_a) down to 1 nm on electroless nickel-plated optical dies while removing the diamond turning marks. Super-finished anisotropic surface texture of 0.28 nm root mean square (RMS) value was obtained for future hard X-ray telescopes through combining FJP and bonnet polishing by Beaucamp et al. [18].

Recently, Beaucamp et al. [19] introduced ultrasonic cavitation into the FJP process to generate micro-bubbles, and these micro-bubbles can boost the material removal rate by up to 380% without causing any degradation of the surface finish. Cao et al. [20, 21] built a material removal and surface generation model for FJP based on theoretical and experimental studies. Shiou et al. [22] proposed an innovative rotary multi-jet polishing process to improve the surface roughness of Zerodur optical glass. To enhance the polishing efficiency of the FJP without degradation of the surface finish, the authors [23, 24] proposed a multi-jet polishing process. The multi-jet polishing process was also utilized for the fast fabrication of structure array surfaces [25]. Recently, they also built a three-dimensional universal tool influence

function model for FJP, which is able to be used for modeling of vertical impinging mode and oblique impinging mode of FJP [26]. However, our understanding of material removal characteristics and surface generation mechanisms of FJP is far from complete, especially on the effect of the stand-off distance (SOD) to this process, as shown in Fig. 1b. The SOD is one of the key factors affecting the FJP process. Current investigations of the SOD are mainly focused on its material removal rate and surface roughness. Booij [2] only did the experimental research on the effect of SOD to the material removal rate, but no clear relationship was found. Li [27] studied the effect of the SOD on the material removal rate and surface quality of the polished surface. Shi et al. [28] did a study on the effect of SOD on the shape of TIF and material removal rate in FJP. However, little attention was paid to the effect of SOD on the surface topography.

In this paper, a systematic investigation of the effect of SOD in FJP on ductile and brittle materials was carried out. The investigation will not only focus on the material removal rate and surface generation but also pay attention to the effect on the shape of TIF and polished surface topography. It will provide a deeper understanding on the material removal characteristics in fluid jet polishing.

2 Experimental Design

To investigate the effect of the SOD in the FJP process systematically, a series of experiments were conducted on both ductile and brittle materials. Nickel copper (NiCu) alloy is used to signify the ductile metal material, which is one of the important and widely used mold-making materials while BK7 optical glass is used to signify the brittle materials. The experiments were carried out on a ZEEKO IRP200 7-axis polishing machine, as shown in Fig. 2a, which can implement bonnet polishing and fluid jet polishing (Fig. 2b) while Fig. 2c shows the fluid jet pumps out of a nozzle with the diameter of 1.1 mm under the 8 bars of the fluid pressure setting. Two groups of the experiments were designed to

Fig. 2 Snapshots of the experimental device. **a** ZEEKO IRP200 7-axis polishing machine, **b** schematic diagram of the relationship of 7 axes, and **c** snapshot of the fluid jet impinging out of the nozzle
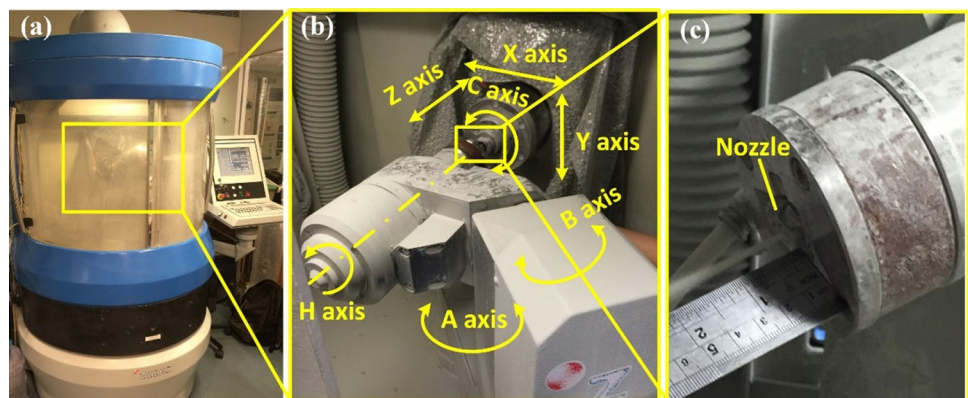
generate the tool influence function (TIF, also called "footprint") on these two materials with various SOD. Table 1 summarizes the polishing conditions. To reduce the effect of the impinging angle, all the experiments adopted 90 degree as the impinging angle. The polishing conditions for these two groups of experiments are the same. To minimize the effect of the initial surface error on the results, single-point diamond turning was conducted on the NiCu surface before the experiment. While the polished BK7 surface was adopted as the workpiece, as shown in Fig. 3. As summarized in Table 1, the SOD varies from 2 to 35 mm, since the fluid flow becomes divergent when the SOD is larger than 35 mm, as shown in Fig. 2c. Three TIFs were generated under each condition for the evaluation. 4000# silicon carbide abrasive (average size is about 3 μm, from FUJIMI Corporation, Japan) was used for the polishing experiments on both NiCu and BK7.

Fig. 3 Snapshots of the workpiece used in this study

3 Results and Discussion

3.1 Analysis of the Effect of the Stand-Off Distance on the TIF Shape

Figures 4 and 5 show the measured contour on Zygo Nexview white light interferometer of the generated TIFs on NiCu and BK7 surfaces, respectively. Their sectional profiles have also been extracted and demonstrated under each TIF contour. The shape of the generated TIFs are almost rotational axisymmetric except for some deviations induced by the wearing of the nozzle. It is interesting to note that the material removal distribution appears to be a ring shape on both NiCu and BK7 with small SOD, and it looks like a "W" shape on its sectional profile. There is almost no material removal at the center of TIF when the SOD is small. With the increase of SOD, the material removal at the center zone also becomes larger gradually. It is interesting to note that the sectional TIF shape changes to a Gaussian-like shape or "U" shape when the SOD is larger than 30 mm in the case of NiCu, which is the deepest at the center and less deep

Table 1 Experimental design

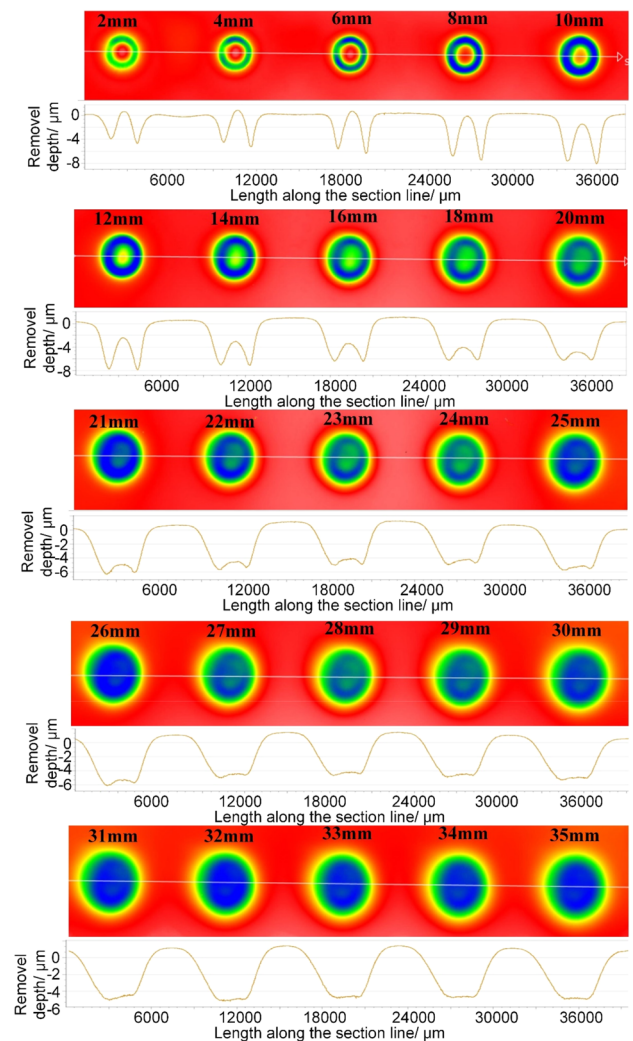| Conditions	Value
Stand-off distance (mm)	2, 4, 6, 8, 10, 12, 14, 16, 18, 20, 21, 22, 23, 24, 25, 26, 27, 28, 29, 30, 31, 32, 33, 34, 35
Fluid pressure (bar)	8
Impinging angle (°)	90
Dwell time (min)	3
Nozzle diameter (mm)	1.1
Polishing slurry	5 wt% 4000# silicon carbide

Fig. 4 Effect of stand-off distance to the shape of tool influence function on nickel copper alloy surface
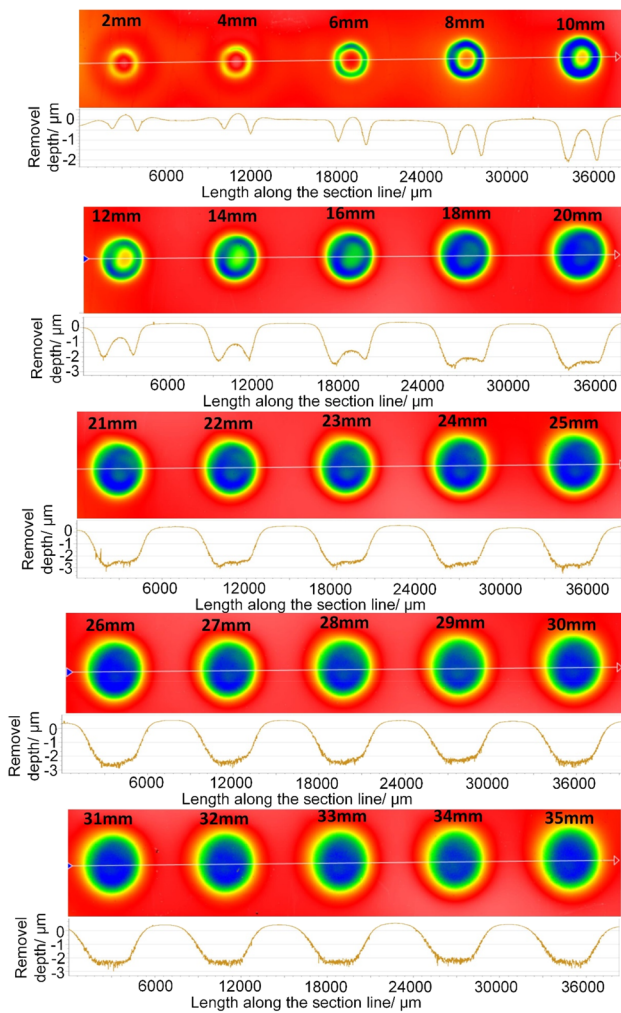
Fig. 5 Effect of stand-off distance to the shape of tool influence function on BK7 optical glass surface
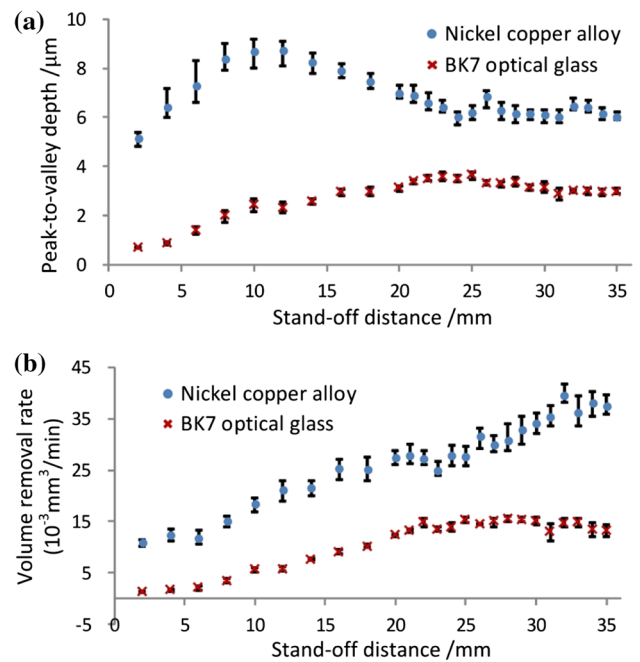

Fig. 6 Effect of the stand-off distance on the material removal rate on different materials in fluid jet polishing: **a** the effect on the peak-to-valley depth of the tool influence function, and **b** the effect on the volume removal rate of the tool influence function

towards the edge. This phenomenon is also observed in the case of BK7 when the SOD is larger than 25 mm.

It is well known that Gaussian-like TIF is conducive to the convergence of the surface form in sub-aperture corrective polishing process [29]. Small SOD (usually smaller than ten times of the nozzle diameter) is usually adopted in practical polishing process, and the sectional TIF is a "W" shape when the nozzle impinges the target surface vertically. Hence, many researchers have started to optimize the TIF shape aiming to obtain Gaussian-like shape through various means. Booij [2] put a stationary helix into the cylindrical nozzle to generate this kind of TIF for the first time, but the fabrication and assembly of this kind of helix is very difficult. Fang et al. [30] attempted to generate the Gaussian-like TIF through oblique impinging the target surface from four or six positions. Li et al. [16] obtained the Gaussian-like TIF through rotating the oblique nozzle. Shi et al. [31] adopted submerged jet polishing to generate Gaussian-like shape

TIF, and implement corrective figuring on optical components successfully. Hence, this study attempts to provide an alternative and simplified way to generate the Gaussian-like shape TIF for FJP.

3.2 Analysis of the Effect of the Stand-Off Distance on the Material Removal Rate

The material removal rate was determined considering the peak-to-valley (PV) depth and volume removal rate (VRR) of the TIF, as shown in Fig. 6. The variation trend of PV and VRR versus SOD are found to be different when polishing on NiCu and BK7, which are ductile and brittle materials, respectively.

In the case of polishing NiCu, the PV value increases with increasing SOD, and reaches the maximum value when the SOD is about 10 mm, as shown in Fig. 6a. The abrasive impacts with each other after gathering inside the nozzle and eject out, leading to energy loss. This is the reason why small PV value of the TIF when the SOD is smaller than around 10 mm. Moreover, when the SOD is around 10 mm, the abrasive velocity becomes the largest, attributing to the largest PV value. The PV value starts to decrease when the SOD is larger than 10 mm until it reaches the minimum at about 23 mm, induced by the obstruction from the surrounding air. When the SOD is larger than 23 mm, the PV value becomes stable. It is interesting to note that the VRR has a

positive relationship to the SOD. With an increase of the SOD, the size of the footprint becomes larger, which leads to the increment of VRR, as shown in Fig. 6b.

In the case of polishing on BK7, both the PV and VRR become larger with increasing SOD until the SOD is about 23 mm. Moreover, both of them start to decrease slightly with a further increase of the SOD. It is different from the trend on NiCu. This phenomenon may can be due to the fact that, when the velocity of abrasive decreases with increasing SOD, and the velocity of some abrasives are not large enough to provide material removal on BK7.

3.3 Analysis of the Effect of the Stand-Off Distance on Surface Topography

Figure 7 shows the measured arithmetic roughness (R_a) of the surface, which varies with the SOD. The arithmetic roughness of the surface was measured by a Zygo Nexview white light interferometer. Considering that the surface roughness at the central zone and circular zone in the generated footprint is different, as shown in Fig. 7a, the surface roughness of these two zones was measured.

For NiCu, it is interesting to note that the SOD has little effect on the surface roughness of the circular zone. The R_a value at the central zone is smaller than that for the circular zone when the SOD is small. Moreover, the R_a value at the central zone becomes larger with increasing SOD until it is equal to the R_a at the circular zone, where SOD is about 12 mm. This is due to the fact that the initial surface roughness is quite small after diamond turning (about 5 nm), and little material removal was generated at the central zone when the SOD is smaller than 12 mm, as shown in Fig. 4. When the SOD is larger than 12 mm, the R_a value at both the circular and central zone of the footprint stop to increase, and converge to a single value (which is 42 nm in this case, with the fluctuation of ± 5 nm), as shown in Fig. 7b.

During the surface generation process, the surface roughness is dominated by the material removal region, which is the circular zone of the TIF. Hence, it infers that the SOD almost has no effect on the surface roughness of NiCu

surface in fluid jet polishing, and it may be the same for other ductile metal surfaces. Table 2 shows the surface topography at the central zone of NiCu measured by the Zygo Nexview white light interferometer and TESCAN VEGA3 scanning electron microscope (SEM). Since NiCu is a ductile material, ductile erosion is the main material removal mechanism, which includes cutting and ploughing, as shown in the SEM results in Table 2. The surface topography is almost the same under different SOD, which corresponds to the surface roughness results, as shown in Fig. 7b.

Hence, a large SOD can be adopted when fluid jet polishing the ductile metal materials as long as the fluid jet is stable. For example, the SOD between 30 mm and 35 mm can be adopted for the polishing of NiCu surface in this study. It can not only implement the highest material removal rate but also generate the Gaussian-like shape TIF.

For BK7, the roughness of the polished surface increases gradually with increasing SOD. Fractures can hardly be seen when the SOD is small, and pits start to come out when the SOD reaches about 12 mm. As shown in Table 3, more and more pits come out when the SOD is larger than 12 mm, which corresponds to the changing trend of the surface roughness. When the SOD is larger than 12 mm, pits are obviously observed, which may be induced by brittle fracture. As shown in Fig. 7b, the growth rate of the R_a value of BK7 is larger than other stages when the SOD is between 12 and 25 mm. This may be explained that there exists the transition stage between ductile material removal and brittle material removal. When the SOD is larger than 25 mm, the material may be mainly removed by brittle removal mode, and the number of fracture cracks increases gradually with a larger SOD, which can be seen from the results obtained by the white light interferometer and the SEM, as shown in Table 3.

When the SOD is smaller than 8 mm, the material may be mainly removed by ductile mode. Hence, the SOD should not be larger than 8 mm under the polishing conditions in this study. Moreover, there may be small differences of this value under different polishing conditions and for different materials. Even though the TIF shape

Fig. 7 The effect of the stand-off distance to the surface roughness: **a** schematic diagram of the measured area of the arithmetic roughness, and **b** measured results of the arithmetic roughness varies with the stand-off distance
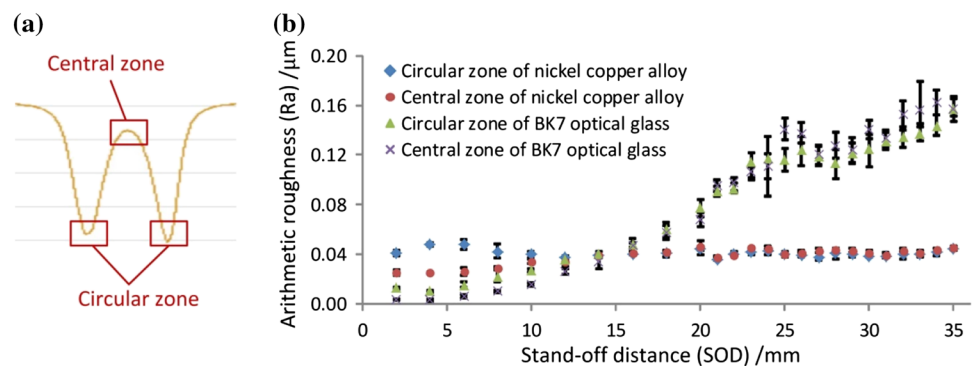
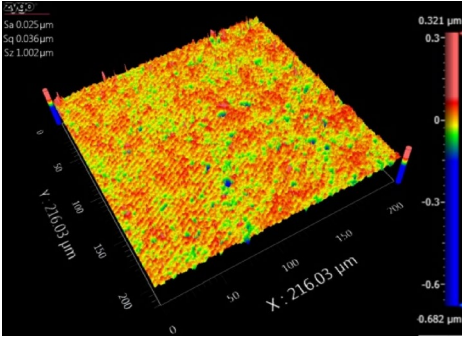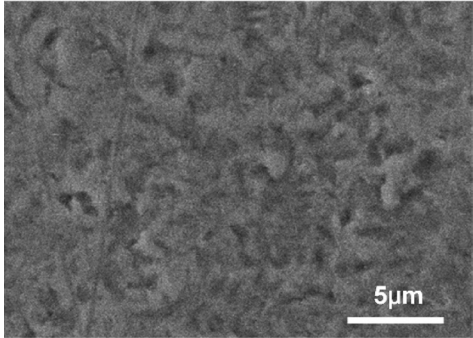**Table 2** Surface topography of the nickel copper alloy varies with the stand-off distance
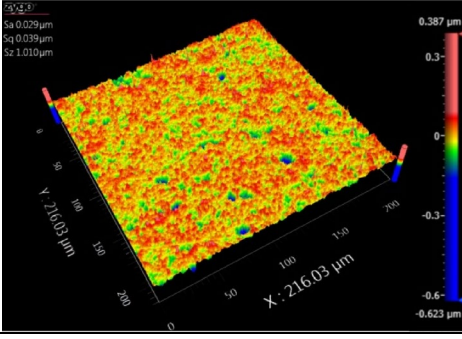
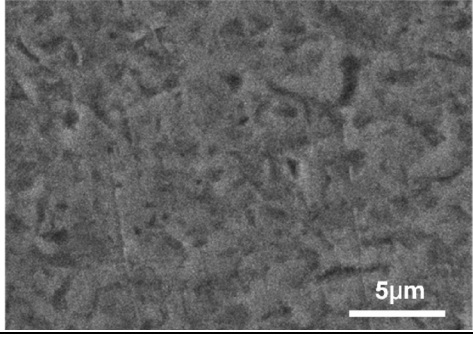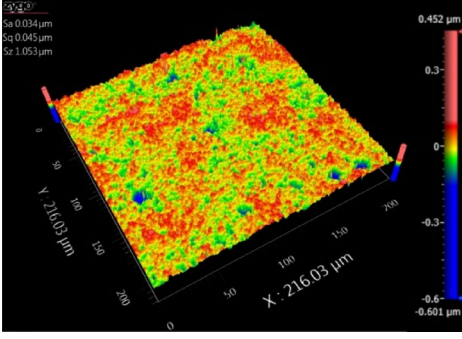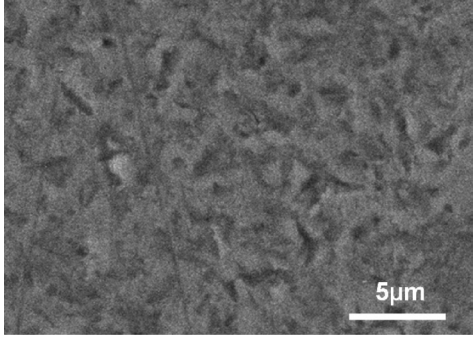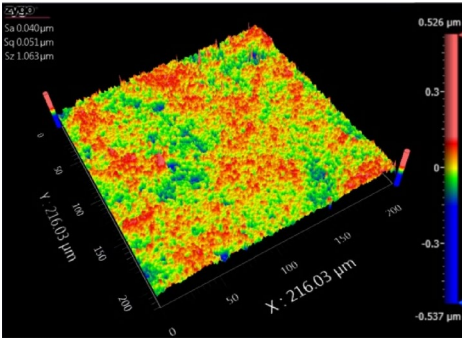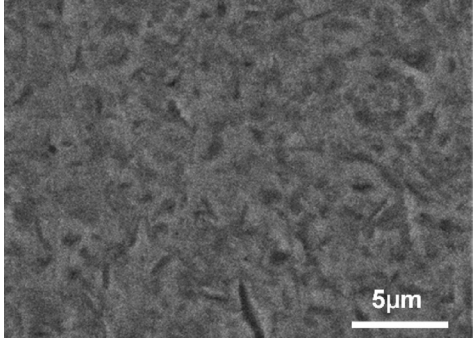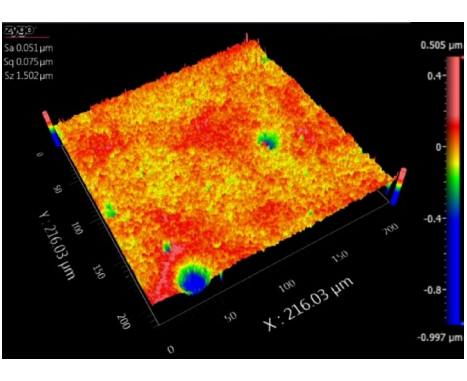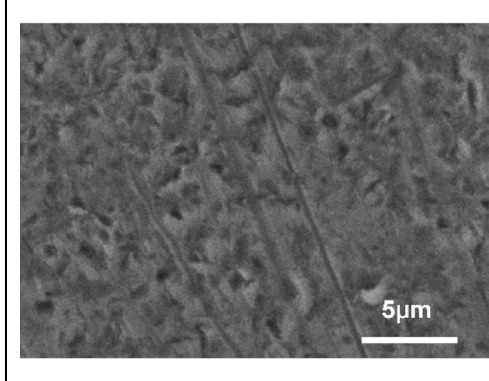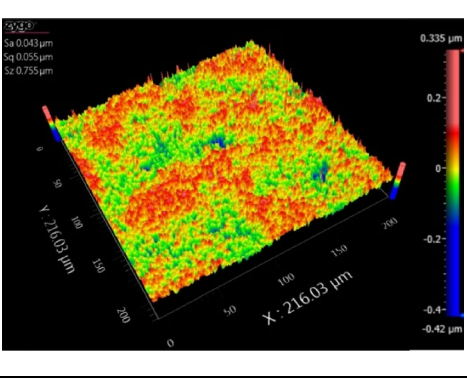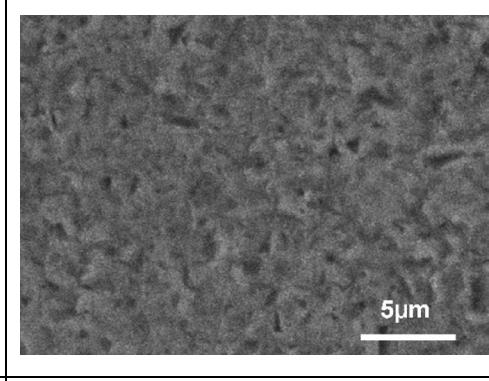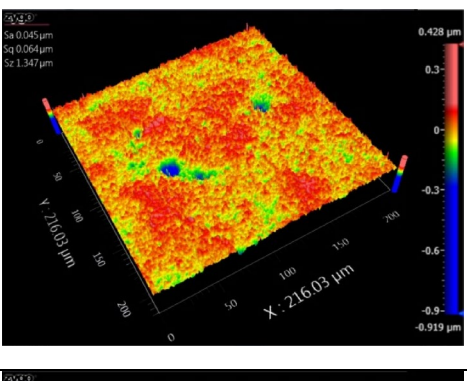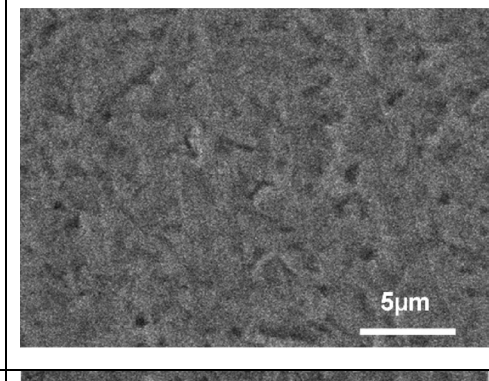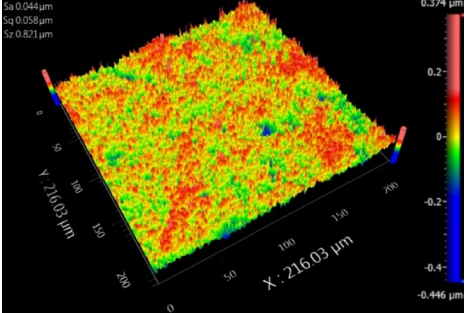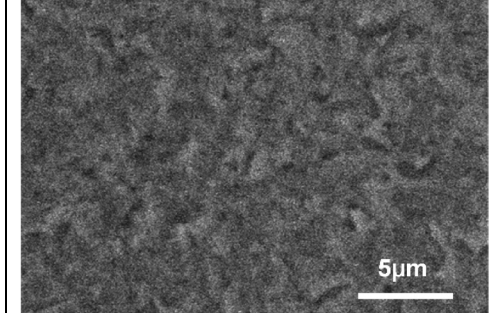| Stand-off distance (mm)	Measured using Zygo Nexview white light interferometer	Measured using TESCAN VEGA3 scan electron microscope
4		
8		
12		
16		

Table 2 (continued)

20		
24		
28		
35		

can also become Gaussian-like shape with large SOD, as shown in Fig. 5, it cannot be used for the polishing of brittle materials because of large surface roughness, which is also observed in the sectional surface profile as shown in Fig. 5.

4 Conclusions

In this study, a systematic investigation of the effect of the stand-off distance (SOD) to the tool influence function and surface topography were carried out in fluid jet polishing

Table 3 Surface topography of the BK7 optical glass varies with the stand-off distance
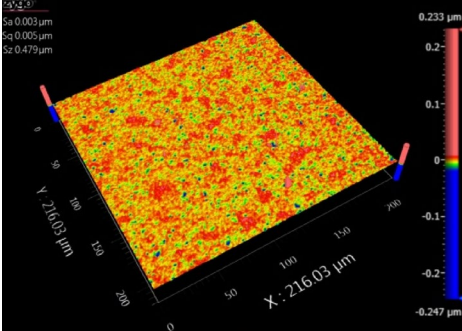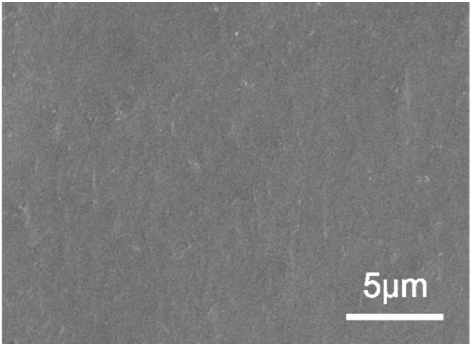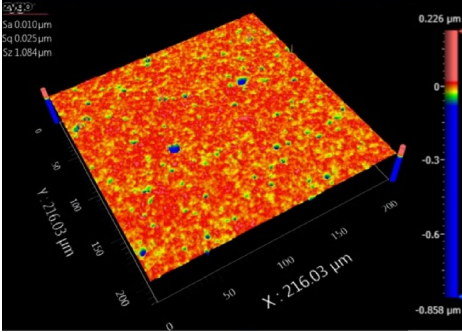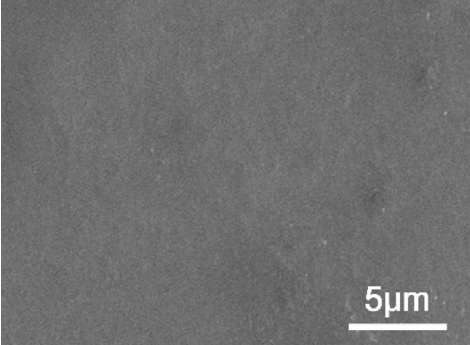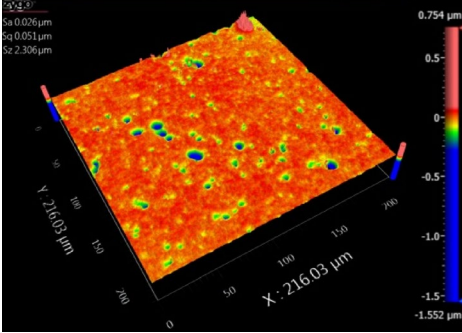
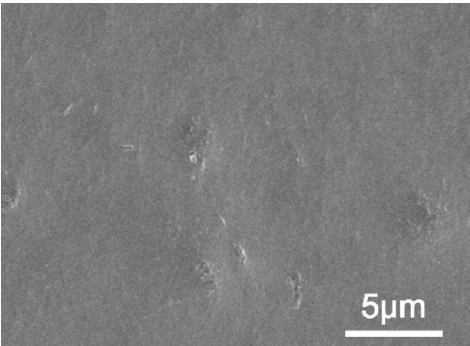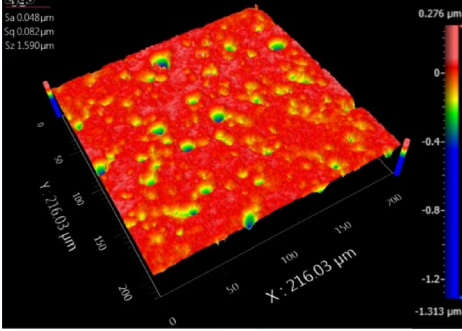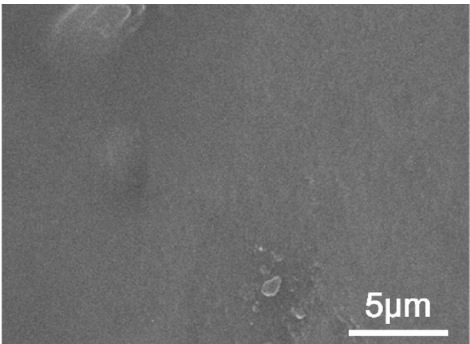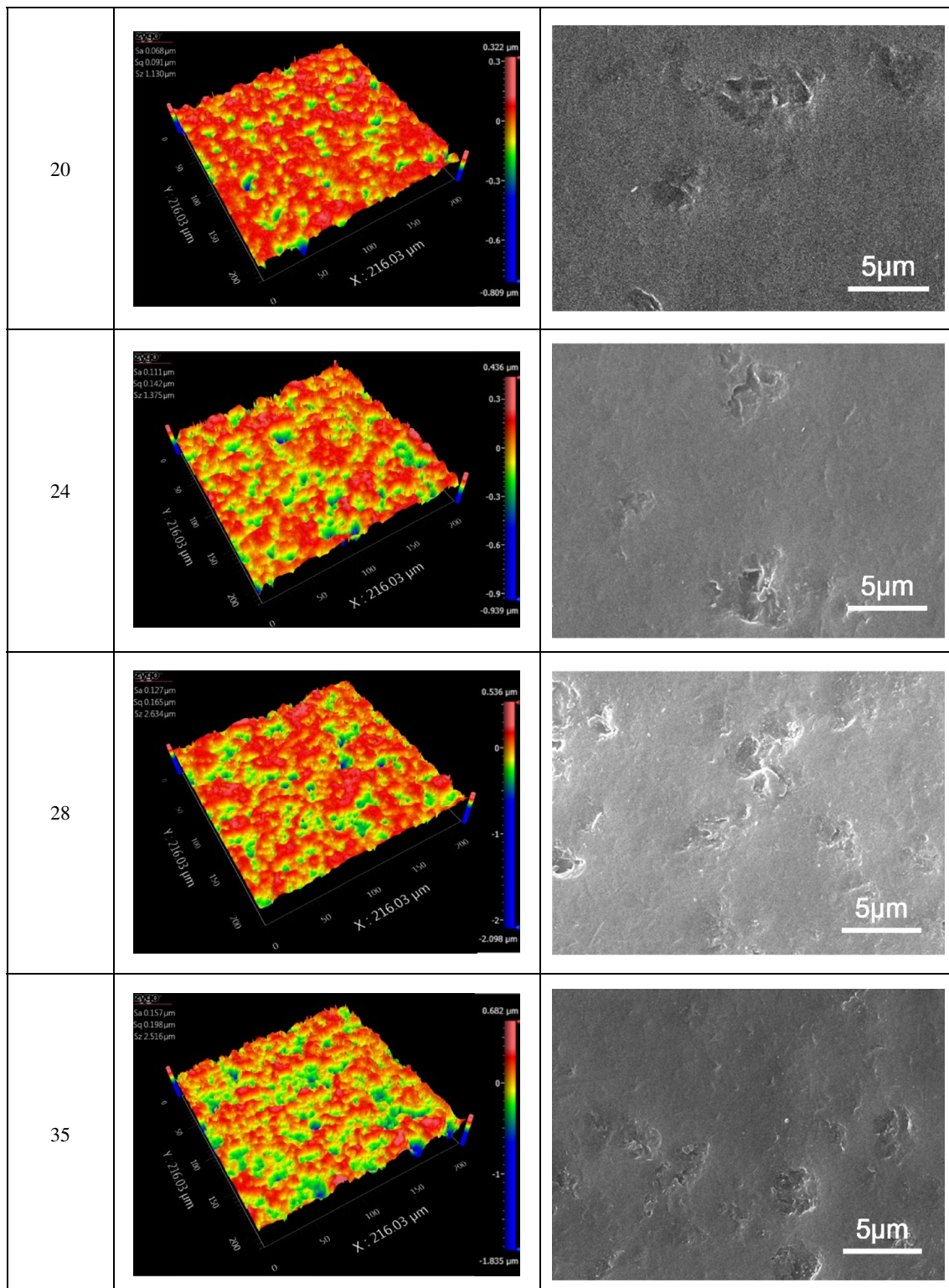| Stand-off distance (mm)	Measured on Zygo Nexview white light interferometer	Measured on TESCAN VEGA3 scan electron microscope
4		
8		
12		
16		

Table 3 (continued)

20	Sa 0.068μm / Sq 0.091μm / Sz 1.130μm — 0.322 μm ... −0.809 μm — X: 216.03 μm, Y: 216.03 μm	5μm
24	Sa 0.111μm / Sq 0.142μm / Sz 1.375μm — 0.436 μm ... −0.939 μm — X: 216.03 μm, Y: 216.03 μm	5μm
28	Sa 0.127μm / Sq 0.165μm / Sz 2.634μm — 0.536 μm ... −2.098 μm — X: 216.03 μm, Y: 216.03 μm	5μm
35	Sa 0.157μm / Sq 0.198μm / Sz 2.516μm — 0.682 μm ... −1.835 μm — X: 216.03 μm, Y: 216.03 μm	5μm

of nickel copper alloy and BK7 optical glass. The following conclusions were made according to the experimental results:

1. The shape of the tool influence function can become Gaussian-like shape from a ring shape with increasing SOD on both ductile and brittle materials.

2. The suitable SOD in FJP is found to be different in polishing of ductile and brittle materials based on the analysis of material removal rate and surface topography. When using a 1.1-mm nozzle provided by Zeeko Ltd., the SOD is preferred to be 25–35 mm for FJP on NiCu, while it is preferred to be ~ 8 mm for FJP on BK7, under the polishing conditions as described in this paper.

3. The material removal mode when polishing on BK7 can be divided into three stages with increasing SOD, which are ductile removal mode, transition mode between ductile and brittle removal mode, and brittle removal mode, respectively. Hence, the SOD should be controlled to be smaller than a certain value so as to pertain ductile material removal mode. This value could be about 8 mm under the polishing conditions, as described in this paper.

4. The conclusions made on NiCu and BK7 may also be suitable for some other ductile materials (e.g., mold steel, nickel, etc.) and brittle materials (e.g., tungsten carbide, sapphire, etc.), respectively. Some certain values described in this paper may be different under different polishing conditions, such as different nozzle diameter, different abrasive size, different fluid pressure, etc.

References

1. Fähnle OW, Van Brug H, Frankena HJ (1998) Fluid jet polishing of optical surfaces. Appl Opt 37(28):6771–6773
2. Booij SM (2003) Fluid jet polishing: possibilities and limitations of a new fabrication technique. PhD Thesis; Technical University of Delft
3. Nouraei H, Kowsari K, Papini M, Spelt JK (2016) Operating parameters to minimize feature size in abrasive slurry jet micromachining. Precis Eng 44:109–123
4. Kowsari K, Schwartzentruber J, Spelt JK, Papini M (2017) Erosive smoothing of abrasive slurry-jet micro-machined channels in glass, PMMA, and sintered ceramics: experiments and roughness model. Precis Eng 49:332–343
5. Axinte DA, Karpuschewski B, Kong MC, Beaucamp AT, Anwar S, Miller D, Petzel M (2014) High energy fluid jet machining (HEFJet-Mach): from scientific and technological advances to niche industrial applications. CIRP Ann Manuf Technol 63(2):751–771
6. Beaucamp A, Namba Y, Freeman R (2012) Dynamic multiphase modeling and optimization of fluid jet polishing process. CIRP Ann Manuf Technol 61(1):315–318
7. Fang F, Zhang N, Guo D, Ehmann K, Cheung B, Liu K, Yamamura K (2019) Towards atomic and close-to-atomic scale manufacturing. Int J Extreme Manuf 1(1):012001
8. Fähnle OW, van Brug H (1999) Finishing of optical materials using fluid jet polishing. In: 14th ASPE annual meeting, pp 509–512
9. Faehnle OW (2012) Abrasive jet polishing approaches to the manufacture of micro-optics with complex shapes. In: Optical Society of America: OM3D-4
10. Faehnle O, Doetz M, Dambon O (2017) Analysis of critical process parameters of ductile mode grinding of brittle materials. Adv Opt Technol 6(5):349–358
11. Booij SM, Fähnle OW, Braat JJ (2004) Shaping with fluid jet polishing by footprint optimization. Appl Opt 43(1):67–69
12. Fang H, Guo P, Yu J (2006) Surface roughness and material removal in fluid jet polishing. Appl Opt 45(17):4012–4019
13. Guo P, Fang H, Yu J (2006) Edge effect in fluid jet polishing. Appl Opt 45(26):6729–6735
14. Tsai FC, Yan BH, Kuan CY, Huang FY (2008) A Taguchi and experimental investigation into the optimal processing conditions for the abrasive jet polishing of SKD61 mold steel. Int J Mach Tools Manuf 48(7):932–945
15. Zhu HT, Huang CZ, Wang J, Li QL, Che CL (2009) Experimental study on abrasive waterjet polishing for hard–brittle materials. Int J Mach Tools Manuf 49(7):569–578
16. Li ZZ, Li SY, Dai YF, Peng XQ (2010) Optimization and application of influence function in abrasive jet polishing. Appl Opt 49(15):2947–2953
17. Li ZZ, Wang JM, Peng XQ, Ho LT, Yin ZQ, Li SY, Cheung CF (2011) Removal of single point diamond-turning marks by abrasive jet polishing. Appl Opt 50(16):2458–2463
18. Beaucamp A, Namba Y (2013) Super-smooth finishing of diamond turned hard X-ray molding dies by combined fluid jet and bonnet polishing. CIRP Ann Manuf Technol 62(1):315–318
19. Beaucamp A, Katsuura T, Kawara Z (2017) A novel ultrasonic cavitation assisted fluid jet polishing system. In: CIRP annals-manufacturing technology
20. Cao ZC, Cheung CF (2014) Theoretical modelling and analysis of the material removal characteristics in fluid jet polishing. Int J Mech Sci 89:158–166
21. Cao ZC, Cheung CF, Ren M (2016) Modelling and characterization of surface generation in Fluid Jet Polishing. Precis Eng 43:406–417
22. Shiou FJ, Asmare A (2015) Parameters optimization on surface roughness improvement of Zerodur optical glass using an innovative rotary abrasive fluid multi-jet polishing process. Precis Eng 42:93–100
23. Wang CJ, Cheung CF, Ho LT, Liu MY, Lee WB (2017) A novel multi-jet polishing process and tool for high-efficiency polishing. Int J Mach Tools Manuf 115:60–73

24. Cheung CF, Wang C, Ho LT, Chen J (2018) Curvature-adaptive multi-jet polishing of freeform surfaces. CIRP Ann 67(1):357–360
25. Wang CJ, Cheung CF, Liu MY, Lee WB (2017) Fluid jet-array parallel machining of optical microstructure array surfaces. Opt Express 25:22710–22725
26. Wang CJ, Cheung CF, Liu MY (2017) Numerical modeling and experimentation of three-dimensional material removal characteristics in fluid jet polishing. Int J Mech Sci 133:568–577
27. Li ZZ (2011) Study on abrasive jet polishing technology. PhD thesis 2011, National University of Defense Technology, Changsha, China
28. Shi CY, Yuan JH, Wu F, Wan YJ (2011) Influence of standoff distance on material removal function in fluid jet polishing. Infrared Laser Eng 4:028
29. Ke XL, Wang CJ, Guo YB, Xu Q (2016) Modeling of tool influence function for high-efficiency polishing. Int J Adv Manuf Technol 84:2479–2489
30. Fang H, Guo P, Yu J (2006) Optimization of the material removal in fluid jet polishing. Opt Eng 45(5):053401
31. Shi C, Yuan J, Wu F, Wan Y (2011) Ultra-precision figuring using submerged jet polishing. Chin Opt Lett 9(9):092201

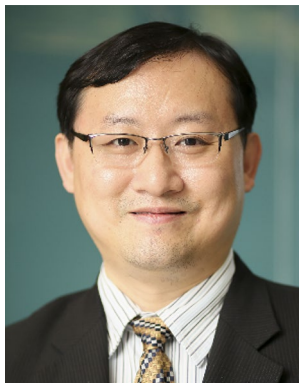Council Member of the International Academy of Engineering and Technology (AET).

Lai Ting Ho is a project officer in the State Key Laboratory of Ultraprecision Machining Technology and the Department of Industrial and Systems Engineering in The Hong Kong Polytechnic University. She received the PhD degree at the Department of Industrial and Systems Engineering of The Hong Kong Polytechnic University in 2015. Her research interest mainly focuses on ultra-precision polishing.
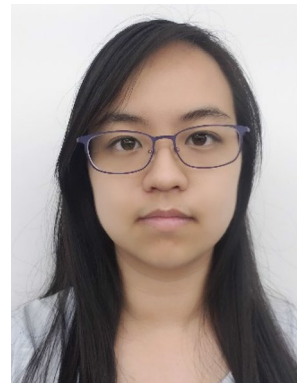
Yee Man Loh is a research assistant in the State Key Laboratory of Ultraprecision Machining Technology and the Department of Industrial and Systems Engineering in The Hong Kong Polytechnic University. She received the Bachelor's degree at the Department of Industrial and Systems Engineering of The Hong Kong Polytechnic University in 2019. Her research interest focuses on ultra-precision polishing technology.

Chunjin Wang a research fellow in the State Key Laboratory of Ultraprecision Machining Technology and the Department of Industrial and Systems Engineering in The Hong Kong Polytechnic University. He received the PhD degree from Xiamen University in 2015. His main research interest focuses on ultra-precision machining technology.

Benny Chi Fai Cheung is a Professor and the Head of the State Key Laboratory of Ultra-precision Machining Technology at the Department of Industrial and Systems Engineering of The Hong Kong Polytechnic University. His research interests include ultra-precision machining, precision metrology, advanced optics manufacturing, etc. He has authored and co-authored more than 260 refereed journal papers. Currently, he is a Board Member of the Asian Society for Precision Engineering and Nanotechnology (ASPEN), an Associate Member of the International Academy for Production Engineering (CIRP), a Fellow and